Redundant MEMS-IMU integrated with GPS for Performance Assessment in Sports

Adrian Waegli, Stéphane Guerrier, Jan Skaloud
Geodetic Engineering Laboratory
École Polytechnique Fédérale de Lausanne, Switzerland

Abstract - In this article, we investigate two different algorithms for the integration of GPS with redundant MEMS-IMUs. Firstly, the inertial measurements are combined in the observation space to generate a synthetic set of data which is then integrated with GPS by the standard algorithms. In the second approach, the method of strapdown navigation needs to be adapted in order to account for the redundant measurements. Both methods are evaluated in experiments where redundant MEMS-IMUs are fixed in different geometries: orthogonally-redundant and skew-redundant IMUs. For the latter configuration, the performance improvement using a synthetic IMU is shown to be 30% on the average. The extended mechanization approach provides slightly better results (about 45% improvement) as the systematic errors of the individual sensors are considered separately rather than their fusion when forming compound measurements. The maximum errors are shown to be reduced even by a factor of 2.

I. INTRODUCTION

This research is part of larger investigations that aim to develop of a low-cost GPS/INS system for performance analysis in sports [1-5]. For ergonomic and economical considerations, we are restricted to the employment of low-cost L1 GPS receivers and Micro-Electro-Mechanical System (MEMS) inertial measurement units (IMU). The performance of our prototype with one MEMS-IMU typically reaches a position accuracy of 0.5m, a velocity accuracy of 0.2m/s and orientation accuracy of 1deg (2deg for heading). Unfortunately, MEMS-IMUs are prone to large systematic errors (e.g. biases, scale factors, drifts) which limit their support in integrated navigation systems. However, they are highly miniaturized and hence the possibility of exploiting numerous MEMS-IMU sensors can be envisaged to enhance the navigation performance.

Skew-redundant IMUs (SRIMUs) are composed of a redundant number of inertial sensors skewed against each other (Fig. 1). Their configuration encapsulates a maximum amount of information depending on the number of sensors and the geometry of configuration. On the other hand, systems based on orthogonally-placed sets of sensors are not optimal in terms of redundancy.

Redundancy can improve the GPS/INS integration performance on several levels. Firstly, direct noise estimation can be achieved directly from the data and the stochastic modeling is closer to reality. Secondly, the noise level can therefore be reduced and defective sensors, spurious signals and sensor malfunctioning can be detected and isolated. Furthermore, sensor error calibration becomes conceivable even during uniform motion or static initialization. Due to the improved navigation accuracy, redundant IMUs bridge the gaps in the GPS data more effectively. Finally, more accurate attitude determination is expected for SRIMU configurations.

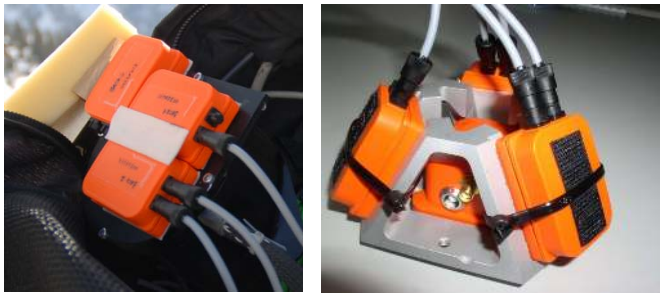

Fig. 1: Orthogonally-redundant (left), skew-redundant IMUs (right).

Redundancy in inertial navigation has been investigated with higher-order IMUs [6]. Several authors have presented results for simulations and emulations, as well as theoretical derivations for MEMS-IMU, but – to the authors' knowledge – no experimental results using MEMS-type sensors have been openly published so far. Based on simulations and theoretical derivations, [7] has found an accuracy improvement of 33% with MEMS-IMUs placed on a tetrahedron. Emulations with MEMS-SRIMU presented by [8] resulted in performance improvements of 20-34%.

In the first part of this article, we investigate the capability of redundant MEMS-IMU sensors to reduce measurement

noise. The parity space method is tested with MEMS-IMU for fault detection and identification algorithm (FDI). Then, we discuss three algorithmic options for the integration of GPS data with redundant MEMS-IMUs. Firstly, the inertial measurements are combined in the observation space to generate a synthetic set of observations that are then integrated by the standard GPS/INS algorithm. In the second approach, the mechanization equations are adapted to account for the redundant measurements. The third algorithm imposes geometrical constraints between the inertial sensors at the update stage. Finally, the performance of the first two algorithms is assessed based on controlled experiments in skiing (orthogonally-redundant IMUs) and motorcycling (skew-redundant IMUs).

II. GPS/INS HARDWARE REDUNDANCY APPROACHES

Redundancy in inertial navigation can be generated at different levels [9]:

- Redundancy at system level (Fig. 2): Several GPS/INS components are formed and processed individually. Fault detection is applied on the resulting navigation solutions.
- Redundancy at sensor level: on IMU (Fig. 3) or multi-IMU level (Fig. 4). In the first geometry, individual IMUs are processed together or individually. Fault detection algorithms can be used before or after the navigation processing. In the second configuration, a multi-IMU sensor (e.g. SRIMU) is processed in one or multiple navigation processors. Fault detection is generally performed before the navigation process.

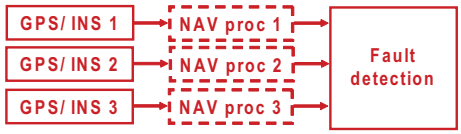

Fig. 2: Redundancy at system level.

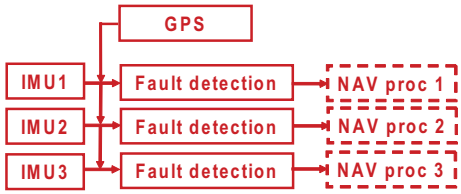

Fig. 3: Redundancy on IMU level.

System redundancy is not attractive for the sports application in terms of cost and size. Therefore, we will concentrate on sensor redundancy and investigate how it can be used to reduce measurement noise and improve navigation accuracy. Furthermore, we focus on detection and isolation of spurious signals and defective sensors. Finally, we highlight two geometries for IMU sensor redundancy (orthogonally- and skew-redundant IMU).

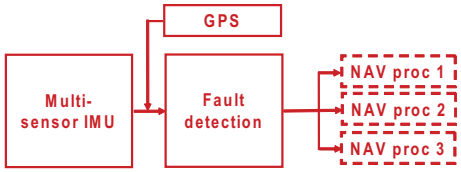

Fig. 4: Redundancy on multi-IMU level.

A. *Noise Reduction*

Combinations of redundant inertial sensors not only decrease the measurement noise, but also offer the possibility to estimate its level during the processing. Hence, the noise figures can evolve during the processing and adapt to particular situations (e.g. increased vibrations).

From n independent measurements $x_1,\ldots,x_n$ (with their respective variances $\sigma_1^2,\ldots,\sigma_n^2$), we can compute their best estimate $\hat{x}$. Assuming homogenous measurements (constant σ_i), its variance $\sigma_{\hat{x}}^2$ can be derived as [10]:

$$\sigma_{\hat{x}} = \sqrt{\sum_{i=1}^{n} w_i^2 \sigma_i^2} = \frac{\sigma_x}{\sqrt{n}} \qquad (1)$$

where the w_i are weighting factors.

According to equation (1), the noise affecting the best estimate $\hat{x}$ derived from measurements of 4 MEMS-IMUs is supposed to be 2 times lower than the noise of the individual MEMS-IMU. Hence, the expected noise reduction for such configuration is of 100%.

The theoretical noise reduction was verified by comparing the differences between the MEMS-IMUs measurements and their best estimate to the reference measurements provided by a tactical-grade IMU (LN200). Thereafter, a parametric compensation was performed to remove systematic errors. Thus, the remaining differences were considered to be composed of white noise only. The averaged noise of the 4 MEMS-IMUs gyros was estimated to 0.0194rad/s, whereas the noise level of their best estimate amounts to 0.0101rad/s. Hence, the experimental noise reduction is of approximately 92 % which confirms the validity of the theoretical model. Fig. 5 illustrates these results graphically.

B. *Fault Detection and Isolation*

Fault Detection and Isolation (FDI) algorithms for inertial navigation were thoroughly investigated in the past. The most commonly used approach is the parity space method [7, 11-13], but other approaches such as artificial neural networks have also been examined [14]. The complexity of

implementation of an efficient FDI system is increased using MEMS-type IMUs. Indeed, their poor performance (noise density variations) creates high risk of false alarm as well as increased exposure to misdetection of faulty measurements [7]. In this article, we investigate the feasibility of using the parity space method with MEMS-IMUs.

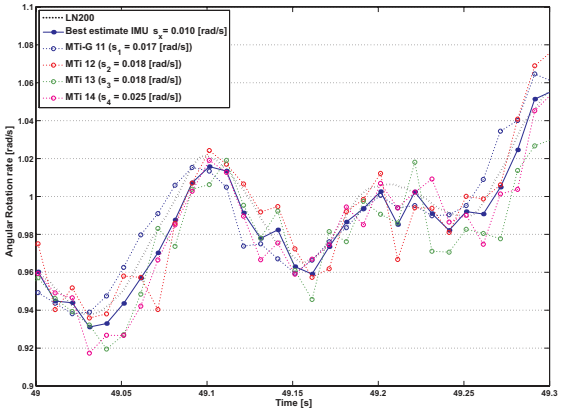

Fig. 5: Illustration of the angular rate measurements of 4 MEMS-IMU in comparison to the reference measurements from a tactical-grade IMU.

This method performs composite statistical tests. Indeed, the fault detection can be viewed as a choice between two hypotheses concerning the absence or the presence of erroneous measurements. The hypothesis test is based on a decision variable D that is compared to a threshold variable T. The decision variable D is computed as follows [12]:

$$D = \mathbf{f}^T \mathbf{f}$$
$$\mathbf{f} = \left[\mathbf{I}_M - \mathbf{A}_\omega \left(\mathbf{A}_\omega{}^T \mathbf{A}_\omega \right)^{-1} \mathbf{A}_\omega{}^T \right] \cdot \mathbf{z} \quad (2)$$

where $M = 12$ is the number of measurements, $N = 3$ is the number of independent parameters, $\mathbf{A}_\omega$ the matrix which transforms the state space to the measurement space (equation (8)) and $\mathbf{z}$ represents the vector of measurements.

The threshold T can be obtained from

$$T\left(P_{FA}, r, \sigma_n^2\right) = \sigma_n^2 \cdot Q^{-1}\left(P_{FA} \middle| r\right) \quad (3)$$

where P_{FA} is the probability of false alarm, $r = M - N$ is the redundancy, $Q\left(\chi^2 \middle| r\right) = 1 - P\left(\chi^2 \middle| r\right)$, $P\left(\chi^2 \middle| r\right)$ being a chi-square probability function, and σ_n^2 is the measurement noise (0.1 rad/s/sqrt(Hz)). Assuming a probability of false alarm of 5% ($P_{FA} = 0.05$), the threshold value for our system is:

$$T\left(P_{FA} = 0.05\right) = 0.0155 rad^2 / s^2$$

We now want to compare this theoretical threshold to an optimized threshold that minimizes the sum of the probability of false alarm and of misdetection [15] and that takes into account the reference measurements provided by the tactical-grade IMU. Comparing the MEMS-IMU measurements to the reference measurements, we first verify the normality of the difference vectors (Fig. 6). It reveals quasi-Gaussian distribution.

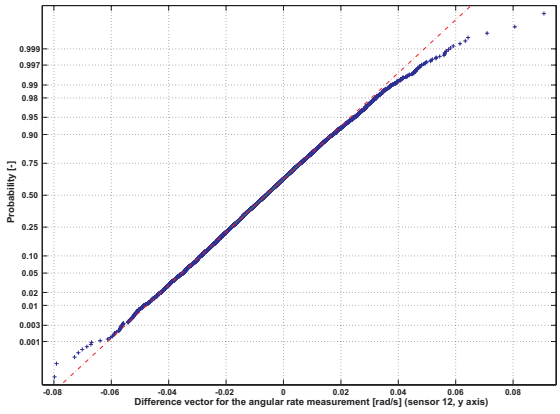

Fig. 6: Graphical assessment of the normality of the difference vector.

Now, we compute the variance of the difference vectors σ_{diff}^2. Assuming that all measurements having a difference exceeding a threshold of $3.5 \cdot \sigma_{diff}$ are erroneous, we estimate the value of $\hat{T}$ that minimizes the sum of false alarms and misdetections ($\hat{T} = 0.0156 rad^2 / s^2$). Thus, we observe that the theoretical threshold values computed with the parity space method and the empirical best threshold value are of the same order of magnitude.

This experimentally derived $\hat{T}$ value could be used in the future data sets. Fig. 7 represents the values of D and T and shows when fault and correct measurements were detected successfully as well as the occurrence of misdetections and false alarms. Nevertheless, the figure also shows the difficulty of finding a good threshold value. Indeed, even with the best possible $\hat{T}$ value approximately 76% of the faults aren't detected. The number of false alarms is also important; the false-alarm-to-fault ratio is roughly 35%. This it shows the need for a more complex FDI model. One possibility would be to train an artificial neural network with a large number of real or emulated measurements in which faults occurs frequently. The presented study considered only fault detection. Similar studies are planned on fault identification.

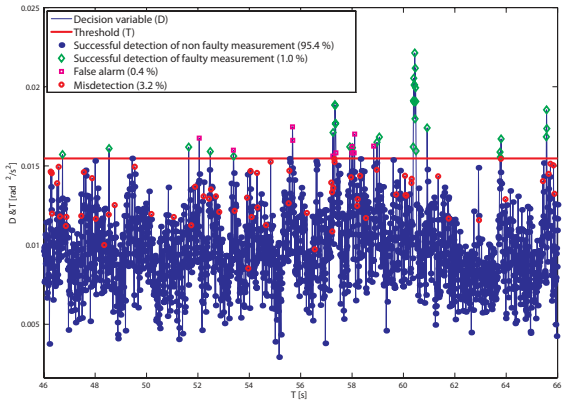

Fig. 7: Estimation of the best threshold and evaluation of its performance.

C. *Redundant IMU Geometries*

Two configurations for redundant IMUs are considered:

- Orthogonally redundant IMUs
- Skew redundant IMUs (SRIMUs)

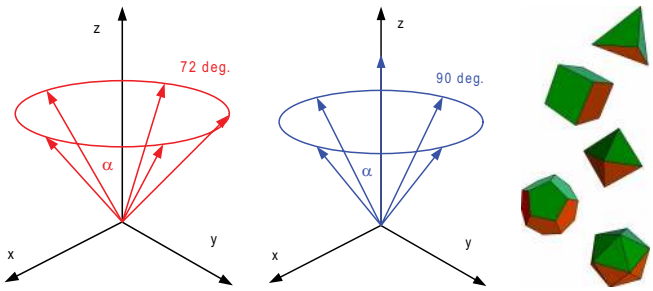

Fig. 8: Inertial sensors placed on a cone (left), on a cone and its axis (middle) and platonic solids (right).

The maximum amount of information – and hence redundancy – is encapsulated in SRIMU systems if the individual sensors are arranged according to well-defined geometries [8, 12, 16]. Ref. [16] presented first a theory how sensors have to be placed on a cone (and eventually its axis) in order to maximize redundancy (Fig. 8). Other configurations that have been considered are based on platonic solids [7]. The first approach presents the advantage that the amount of redundancy of the vertical axis can be varied with respect to the redundancy of the horizontal plane by changing the cone's half-angle. This is an interesting option when IMU are used together with GPS, because the vertical performance is reduced by a factor 2-3 with respect to the horizontal plane due to the satellite geometry. However, the motion of athletes is complex and involves large rotations around all axes. Hence, the approach using platonic solids, e.g. a tetrahedron, seems appropriate.

III. SYSTEM AND OBSERVATION MODEL

In this section, we will first present the mechanization approach applied for the integration of GPS with single IMUs. Then, three mechanizations approaches described by [6] are reviewed.

A. *Single IMU Mechanization*

An extended Kalman filter (EKF) has been implemented in the local level frame (superscript n) which makes the interpretation of the state variables straightforward. The following strapdown equations need to be solved [10]:

$$\begin{bmatrix} \dot{\mathbf{r}}^n \\ \dot{\mathbf{v}}^n \\ \dot{\mathbf{R}}_b^n \end{bmatrix} = \begin{bmatrix} \mathbf{v}^n \\ \mathbf{R}_b^n \mathbf{f}^b - \left(\boldsymbol{\omega}_{in}^n + \boldsymbol{\omega}_{ie}^n\right) \times \mathbf{v}^n + \mathbf{g}^n \\ \mathbf{R}_b^n \left(\boldsymbol{\omega}_{ib}^b - \boldsymbol{\omega}_{in}^b\right) \end{bmatrix} \tag{4}$$

Given the observations $\boldsymbol{\omega}_{ib}^b$ and $\mathbf{f}^b$, knowledge of $\mathbf{g}^n$, and the initial conditions.

For the inertial measurements a simplified model was considered. Judging that the misalignments, drifts and constant offsets could not be decorrelated efficiently given the characteristics of the MEMS-IMU sensors and limited integration periods, only a bias term is considered [5]. Their associated errors are modeled as first order Gauss-Markov processes:

$$\begin{aligned} \hat{\ell}^b &= \ell^b + \mathbf{b}_{\ell^b} + \mathbf{w}_{\ell^b} \\ \dot{\mathbf{b}}_{\ell^b} &= -\beta_{\ell^b} \cdot \mathbf{b}_{\ell^b} + \sqrt{2\sigma_{\ell^b}^2 \beta_{\ell^b}} \cdot \mathbf{w}_{\ell^b} \end{aligned} \tag{5}$$

where $\hat{\ell}^b$ is the estimated inertial observation (specific force $\mathbf{f}^b$ or rotation rate $\boldsymbol{\omega}_{ib}^b$), ℓ^b the inertial measurement, $\mathbf{b}_{\ell^b}$ the bias of the inertial measurement, $\mathbf{w}_{\ell^b}$ the measurement noise, $\sigma_{\ell^b}^2$ the covariance at zero time lag and β_{ℓ^b} the inverse of the correlation time [17].

B. *Synthetic Mechanization*

In the synthetic mechanization approach, the redundant IMU data is merged before being introduced to GPS/INS algorithm based on the single IMU mechanization (Fig. 9). While fusing the IMU data, defective sensors can be detected and realistic noise and covariance terms can be estimated [6]. However, the estimated "compound" biases cannot be back-projected to the individual sensors.

In a first step, synthetic inertial measurements $\boldsymbol{\omega}^b$ and $\mathbf{f}^b$ need to be generated:

$$\boldsymbol{\omega}^b = \boldsymbol{\pi}_\omega \boldsymbol{\ell}_\omega$$
$$\mathbf{f}^b = \boldsymbol{\pi}_f \boldsymbol{\ell}_\mathbf{f} \tag{6}$$

This requires estimating the orthogonal projectors $\boldsymbol{\pi}_\omega$ for the angular rate measurements $\boldsymbol{\ell}_\omega$ and $\boldsymbol{\pi}_f$ for the specific force $\boldsymbol{\ell}_\mathbf{f}$ as well as their accuracy ($\mathbf{P}_{\boldsymbol{\omega}^b}$ and $\mathbf{P}_{\mathbf{f}^b}$):

$$\begin{aligned}
\boldsymbol{\pi}_\omega &= \left(\mathbf{A}_\omega^T \mathbf{P}_{\boldsymbol{\ell}_\omega} \mathbf{A}_\omega\right)^{-1} \mathbf{A}_\omega^T \mathbf{P}_{\boldsymbol{\ell}_\omega} \\
\boldsymbol{\pi}_f &= \left(\mathbf{A}_f^T \mathbf{P}_{\boldsymbol{\ell}_\mathbf{f}} \mathbf{A}_f\right)^{-1} \mathbf{A}_f^T \mathbf{P}_{\boldsymbol{\ell}_\mathbf{f}} \\
\mathbf{P}_{\boldsymbol{\omega}^b} &= \mathbf{A}_\omega^T \mathbf{P}_{\boldsymbol{\ell}_\omega} \mathbf{A}_\omega \\
\mathbf{P}_{\mathbf{f}^b} &= \mathbf{A}_f^T \mathbf{P}_{\boldsymbol{\ell}_\mathbf{f}} \mathbf{A}_f
\end{aligned} \tag{7}$$

$\mathbf{A}_\omega$ and $\mathbf{A}_f$ transform the data from the actual sensor axes (superscript b_i) to the three orthogonal axes of the predefined body frame (superscript b). Their rows contain the direction cosine matrices of the angular rate sensor and accelerometer axes:

$$\mathbf{A}_\omega = \begin{bmatrix} \mathbf{R}_b^{b_{\omega 1}} \\ \cdots \\ \mathbf{R}_b^{b_{\omega i}} \\ \cdots \\ \mathbf{R}_b^{b_{\omega n}} \end{bmatrix} \qquad \mathbf{A}_f = \begin{bmatrix} \mathbf{R}_b^{b_{f 1}} \\ \cdots \\ \mathbf{R}_b^{b_{f i}} \\ \cdots \\ \mathbf{R}_b^{b_{f n}} \end{bmatrix} \tag{8}$$

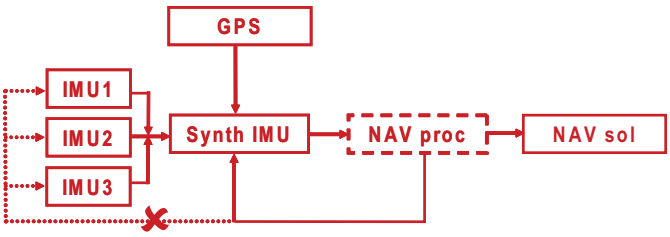

Fig. 9: Principle of mechanization based on a synthetic IMU.

C. *Extended Mechanization*

In order to be able to estimate individual sensor errors, the last two expressions of equation (4) need to be revised:

$$\begin{bmatrix} \dot{\mathbf{r}}^n \\ \dot{\mathbf{v}}^n \\ \dot{\mathbf{R}}_b^n \end{bmatrix} = \begin{bmatrix} \mathbf{v}^n \\ \boldsymbol{\pi}_f \mathbf{R}_b^n \boldsymbol{\ell}_\mathbf{f} - \left(\boldsymbol{\omega}_{in}^n + \boldsymbol{\omega}_{ie}^n\right) \times \mathbf{v}^n + \mathbf{g}^n \\ \mathbf{R}_b^n \left(\boldsymbol{\pi}_\omega \boldsymbol{\ell}_\omega - \boldsymbol{\omega}_{in}^b\right) \end{bmatrix} \tag{9}$$

With this approach, it is possible to detect defective sensors and to estimate noise terms during the integration (Fig. 10). Moreover, the systematic errors can be modeled and estimated for each sensor. However, this approach requires the modification of the GPS/INS software to accommodate the new form of mechanization equations.

D. *Geometrically-Constrained Mechanization*

As for the extended mechanization, the geometrically-constrained mechanization allows estimating the individual sensor errors. In this approach, multiple navigation solutions are computed (one for each IMU) and compared at regular time intervals (Fig. 11). This is, however, at the cost of increased computational effort and important modifications of the GPS/INS software. In principle, defective sensors cannot be detected and realistic noise terms cannot be estimated by this approach.

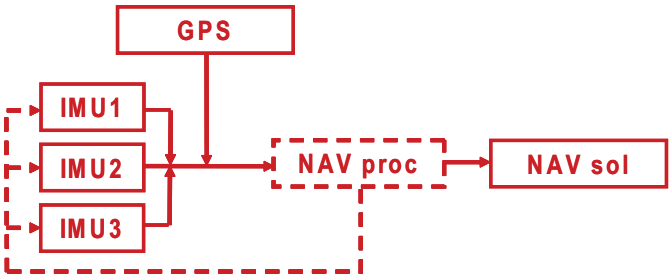

Fig. 10: Principle of extended IMU mechanization.

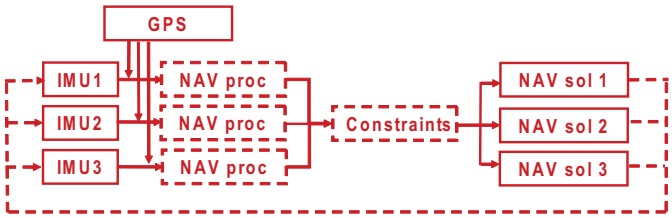

Fig. 11: Principle of geometrically-constrained IMU mechanization.

Consider that two IMUs are employed. Both units are integrated using the standard IMU mechanization. The relative orientation parameters (relative orientation $\mathbf{R}_{b_1}^{b_2}$ and lever arm $\mathbf{a}_{b_1}^{b_2}$) can be modeled and estimated as random constants supposing their direct determination is not accurate enough [6].

$$\begin{aligned}
\dot{\mathbf{R}}_{b_1}^{b_2} &= 0 \\
\dot{\mathbf{a}}_{b_1}^{b_2} &= 0
\end{aligned} \tag{10}$$

At predefined stages, the following relationships can be imposed:

$$\begin{aligned}\mathbf{R}_{b_1}^{n} &= \mathbf{R}_{b_1}^{b_2}\mathbf{R}_{b_2}^{n} \\ \mathbf{r}_1^n &= \mathbf{r}_2^n - \mathbf{R}_{b_1}^{n}\mathbf{a}_{b_1}^{b_2} \\ \mathbf{v}_1^n &= \mathbf{v}_2^n - \left(\Omega_{ni}^{b1} + \Omega_{ib}^{b1} + \Omega^{b1}(\mathbf{b}_\omega)\right)\mathbf{a}_{b_1}^{b_2}\end{aligned} \tag{11}$$

E. *Algorithm Selection*

The derivation of a synthetic IMU is the most straightforward approach as it does not require any modification of the standard GPS/INS algorithm. Unlike the extended and geometrically-constrained method, this approach does not allow the feedback of sensor errors which might yield less optimal navigation performance. On the other hand, [5] has shown that the MEMS-IMU biases are relatively stable for the short trajectories encountered in some sports (e.g. lap, downhill). Furthermore, the same research has shown that the simplified error model was suitable for the considered application and sensors.

The geometrically-constrained approach represents and interesting option for system calibration if the relative sensor geometry is insufficiently known. As mentioned, the computational effort is increased considerably compared to the first two approaches. In addition, it is more sensitive to sensor failures because defects can only be noticed at the update stage and the measurement faults can generally not be isolated. In the sequel, the synthetic IMU approach will be compared to the approach based on extended IMU mechanization.

IV. RESULTS

A. *Estimation of the Relative Alignment of the MEMS-IMU*

The alignment between the individual MEMS-IMU sensors and with respect to the reference IMU was estimated by feeding the EKF with the reference attitude observations using the following model:

$$\begin{aligned}h(\hat{\mathbf{x}}^-) &= (\mathbf{I}_3 + \Omega)\boldsymbol{\varphi}_{LN200} + \mathbf{w}_\varphi \\ \dot{\Omega} &= 0\end{aligned} \tag{12}$$

where Ω is the skew-symmetric form of the misalignment angles, $\boldsymbol{\varphi}_{LN200}$ is the vector of Euler angles of the reference attitude, and $\mathbf{w}_\varphi$ the measurement noise. The accuracy of the determined misalignment angles is limited by the accuracy of the MEMS-IMU determination and is estimated to 0.5°.

B. *Two Orthogonally-Redundant IMU*

In a skiing experiment, the low-cost L1 GPS/MEMS-IMU instruments were mounted in a backpack together with a reference system, comprising a dual-frequency GPS receiver (Javad) and a tactical-grade IMU (LN200). Redundant MEMS-IMU sensors (Xsens MTi) in orthogonal configuration were rigidly fixed to the reference IMU (Fig. 12). A downhill of approximately 1 minute duration was performed by a professional skier after a static initialization phase of 2-3 minutes.

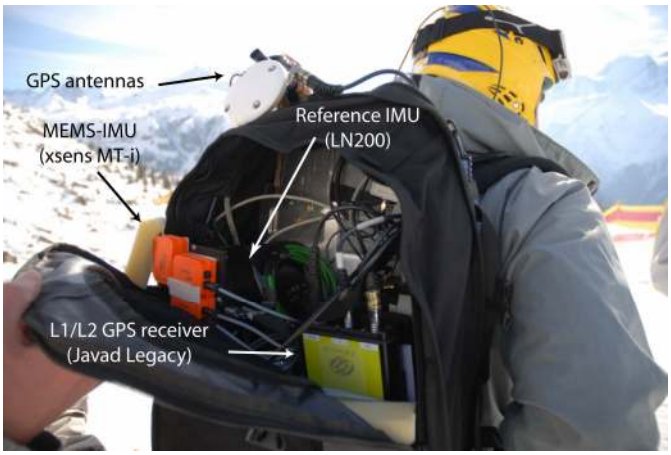

Fig. 12: Investigation of orthogonally redundant IMUs: Experimental setup mounted on a professional skier.

For this experiment, we integrate two orthogonally redundant IMUs at 100Hz with the L1 as well as the L1/L2 DGPS at 1Hz. The use of two MEMS-IMU reduces the noise level of the measurements by a factor of $\sqrt{2}$. In this configuration, measurement outliers can neither be detected nor identified. Nevertheless, an accuracy improvement was noticed for the orientation (20-30%, Table 1) while the position and velocity states where not improved significantly. The performance improvement is similar for the two integration approaches and equivalent with respect to the employment of single- or dual-frequency differential processing.

	L1		L1/L2	
	synthetic	extended	synthetic	extended
roll	-37%	-24%	-43%	-20%
pitch	-25%	-5%	-7%	8%
heading	-34%	-24%	-32%	-22%

Table 1: Orientation improvement with two orthogonally-redundant MEMS-IMUs compared to the average performance of the single sensors.

The estimated synthetic biases represent approximately the average of the biases estimated by processing of the individual MEMS-IMUs (Fig. 13). Ref. [5] has already shown the relevance of using this simplified error model.

C. *Skew-Redundant IMU*

For a second experiment, a regular tetrahedron consisting of 4 Xsens MT-i was set up (Fig. 1). In order to investigate the performance of the multi-IMU system, it was fixed rigidly to a reference system consisting again of a tactical-grade IMU

(LN200) and a differential, dual-frequency GPS receiver (Javad Legacy) [18]. The system was installed on a motorcycle (Fig. 14).

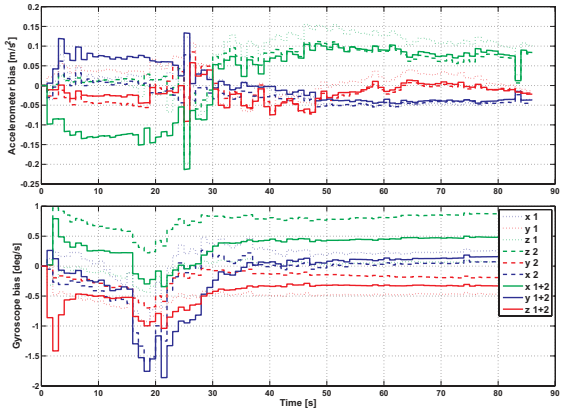

Fig. 13: Synthetic IMU bias compared to the individually estimated biases.

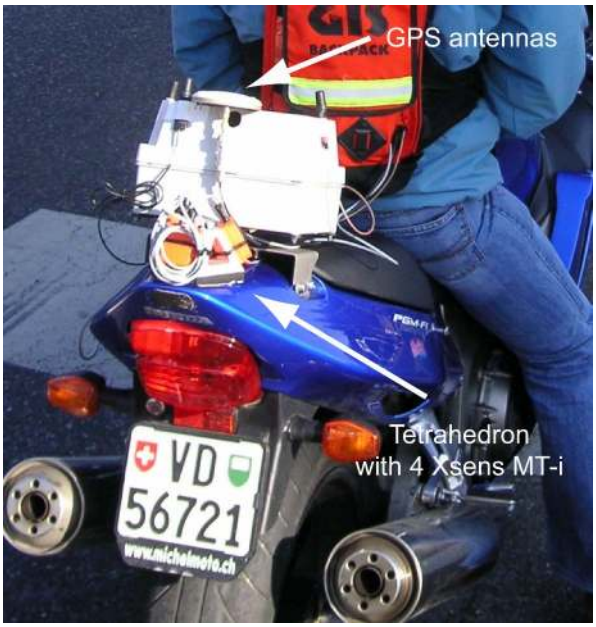

Fig. 14: SRIMU installed on a motorcycle.

As previously shown for this setup, the inertial measurement noise is reduced by a factor of 2 due to the measurement redundancy. Table 2 summarizes the navigation performance of the particular GPS/MEMS-SRIMU system. The orientation accuracy of the system has now dropped below 1deg. The experiment confirms previous findings [4] where the velocity and orientation accuracies were invariant with respect to the accuracy of GPS aiding (e.g. L1 or L1/L2 differential code and carrier-phase). On the other hand, the position accuracy is largely improved using dual-frequency GPS processing with ambiguity fixing. Because of the relatively long baseline for single-frequency CP-DGPS, the ambiguities could not be fixed which resulted in code-differential positioning accuracy.

	synthetic		extended	
	L1	L1/L2	L1	L1/L2
N [m]	0.83	0.03	0.83	0.03
E [m]	2.40	0.05	2.40	0.04
D [m]	0.81	0.08	0.81	0.07
vN [m/s]	0.07	0.05	0.07	0.03
vE [m/s]	0.07	0.07	0.07	0.05
vD [m/s]	0.11	0.10	0.12	0.06
rl [deg]	0.69	1.09	1.04	0.83
pt [deg]	0.79	1.05	0.92	0.86
hd [deg]	0.42	0.68	0.67	0.62

Table 2: Average absolute accuracy of the tested GPS/MEMS-SRIMU system.

Table 3 indicates the performance improvement of the GPS/MEMS-SRIMU system compared to the average accuracy of the solutions computed with the single MEMS-IMUs. An average improvement of 30% is obtained for the synthetic IMU approach. The extended mechanization performs slightly better than the synthetic approach (average improvement of 46%). This can be explained by the estimation of the individual biases and the FDI scheme that can run in parallel to the filter (rather than in cascade as in the synthetic IMU approach). However, the navigation performance is not improved by 100% as could be expected from the noise reduction. Indeed, residual correlations between the inertial measurements as well as the correlations between the filter states most likely limit the accuracy progression.

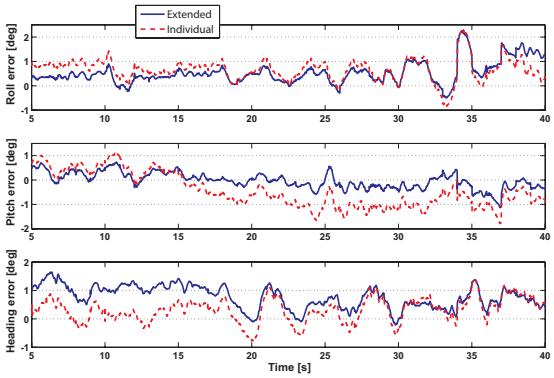

Fig. 15: Orientation error after integration of a single sensor (individual) and after extended mechanization.

Table 3 also recapitulates the performance enhancement with respect to the maximum errors. It is of 61% for the synthetic IMU approach and even more substantial for the extended mechanization where the maximum errors are reduced by a factor of 2. Fig. 15 illustrates how the peaks of

the orientation errors in the single MEMS-IMU/GPS integration are smoothed out by the extended mechanization.

	RMS		Maximum error	
	synthetic	extended	synthetic	extended
N	-29%	-35%	-71%	-94%
E	-41%	-51%	-77%	-94%
D	-5%	-19%	-27%	-82%
vN	-37%	-61%	-82%	-95%
vE	-50%	-67%	-81%	-93%
vD	-7%	-44%	-25%	-74%
rl	-57%	-67%	-80%	-87%
pt	-28%	-41%	-59%	-80%
hd	-21%	-27%	-45%	-69%

Table 3: Performance improvement of the average and maximum errors by the MEMS-SRIMUs compared to the performance of the individually integrated MEMS-IMU sensors.

D. Note on the Observability

The estimated synthetic biases represent again the mean value of the biases estimated individually (similar to those depicted in Fig. 13). On the other hand, the biases estimated in the extended mechanization do not match the individually estimated biases (Fig. 16). The covariance analysis of the state vector reveals that biases are only weakly correlated (0.2-0.3, Fig. 17). The correlation level does not explain the encountered differences and therefore we focus on the observability of the system. A system with system matrix $\mathbf{F}$, observation matrix $\mathbf{H}$ and n states is observable if the observablity matrix $\mathbf{O}$ has rank n [19]:

$$\mathbf{O} = \begin{bmatrix} \mathbf{H} \\ \mathbf{HF} \\ \cdots \\ \mathbf{HF}^{i} \\ \cdots \\ \mathbf{HF}^{n-1} \end{bmatrix} \tag{13}$$

The mechanization approach based on a single MEMS-IMU is observable: the observability matrix has rank 15 which corresponds to the number of states. In the extended mechanization approach, the number of states increases to 33, but the rank of the observability matrix remains 15. Therefore, it might be that the observability of the sensor biases is reduced in favor of the "interesting" states (position, velocity and orientation). In the future, we will concentrate on the observability of the subsystems in order to evaluate possibilities to further improve the extended mechanization approach and to verify its stability. Such analysis could be based on singular value decomposition as suggested in [20]. Indeed, each singular value is an observability measure for the subspace spanned by the corresponding singular vector.

V. CONCLUSION AND PERSPECTIVES

In the first part of the article, we have presented fault detection and identification with the commonly used parity space method in case of redundant MEMS-IMUs. It was shown that the theoretical threshold matched that derived from experimental data. However, the percentages of undetected errors (76%) as well as the level of false alarms (35%) are unacceptable and new methods have to be developed.

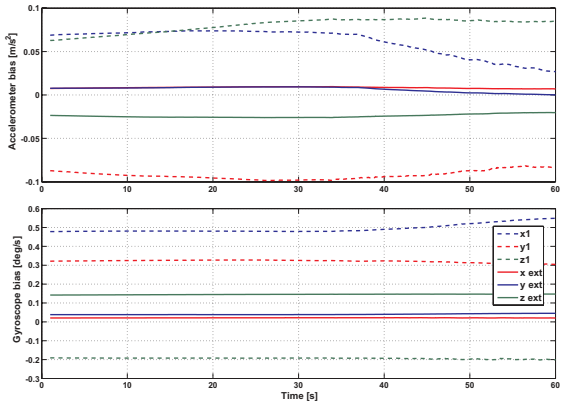

Fig. 16: Individual biases vs. biases estimated by the extended mechanization.

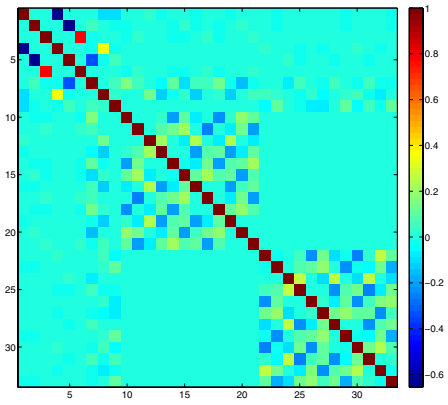

Fig. 17: State correlations in extended mechanization - position (3), velocity (3), orientation (3), accelerometer biases (12), gyroscope biases (12).

In the second part, we focused on the method of integration of redundant MEMS-IMU with GPS data. We have shown that the navigation performance can be improved by 30-50% when using 4 MEMS-IMUs placed on the faces of a regular tetrahedron. Maximum errors can even be reduced by a factor of 2. The skew-redundant geometry makes maximum use of the available information. Two integration approaches were been investigated: an algorithm based on a synthetic IMU and an extended mechanization approach, where the state vector

is increased by individual biases per sensor. The second method is found to be more optimal for system calibration because the error characteristics of the individual sensors are considered separately rather than the fusion of compound measurements. Furthermore, fault detection can be performed within this integration procedure whereas the synthetic approach requires cascade processing. Although it performs slightly better than the first approach, it was shown that the estimated biases do not correspond to the real biases. This might be explained by the reduced observability of the system, but this hypothesis needs further investigation in order to assess the entire potential of the extended mechanization.

Due to the increased accuracy and the possibility to detect measurement errors, redundant IMUs have the potential of better bridging the gaps in GPS data. Future work will include additional experiments to confirm the accuracy improvements of the two presented experiments. More testing and simulations are required in order to determine the ideal number and geometry of the redundant IMUs. Furthermore, we aim to focus on alternative approaches to improve static initialization.

ACKNOWLEDGEMENT

This research is financed by TracEdge, based at Grenoble, France.

Special thanks to Dr. Ismael Colomina from Institut de Geomatica, Castelldefels, Spain, for sharing his ideas and encouraging this research. Thanks to Stéphane Beauregard for reviewing the article.

REFERENCES

[1] A. Waegli, F. Meyer, S. Ducret, J. Skaloud, and R. Pesty, "Assessment of Timing and Performance Based on Trajectories from low-cost GPS/INS Positioning," in *4th International Congress on Science and Skiing*, St. Christoph, Austria, 2007.

[2] A. Waegli, A. Schorderet, C. Prongué, and J. Skaloud, "Accurate Trajectory and Orientation of a Motorcycle derived from low-cost Satellite and Inertial Measurement Systems," in *7th ISEA Conference 2008*, Biarritz, France, 2008.

[3] A. Waegli and J. Skaloud, "Turning Point – Trajectory Analysis for Skiers," *InsideGNSS,* 2007.

[4] A. Waegli and J. Skaloud, "Assessment of GPS/MEMS-IMU Integration Performance in Ski Racing," in *ENC*, Geneva, Switzerland, 2007.

[5] A. Waegli, J. Skaloud, P. Tomé, and J.-M. Bonnaz, "Assessment of the Integration Strategy between GPS and Body-Worn MEMS Sensors with Application to Sports," in *ION GNSS*, Fort Worth, Texas, 2007.

[6] I. Colomina, M. Giménez, J. J. Rosales, M. Wis, A. Gómez, and P. Miguelsanz, "Redundant IMUs for Precise Trajectory Determination," in *XXth ISPRS Congress* Istanbul, 2004.

[7] S. Sukkarieh, P. Gibbens, B. Brocholsky, K. Willis, and H. F. Durrant-Whyte, "A Low-Cost Redundant Inertial Measurement Unit for Unmanned Air Vehicles," *The International Journal of Robotics Research,* vol. 19, p. 1089, 2000.

[8] A. Osman, B. Wright, S. Nassar, A. Noureldin, and N. El-Sheimy, "Multi-Sensor Inertial Navigation Systems Employing Skewed Redundant Inertial Sensors," in *ION GNSS 19th International Technical Meeting of the Satellite Division*, Fort Worth, TX, 2006.

[9] D. J. Allerton and H. Jia, "A Review of Multisensor Fusion Methodologies for Aircraft Navigation Systems," *The Journal of Navigation,* vol. 58, pp. 405-417, 2005.

[10] D. H. Titterton and J. L. Weston, *Strapdown inertial navigation technology*: Peter Peregrinus Ltd, 1997.

[11] E. Gai, J. V. Harrison, and K. C. Daly, "Generalized Likelihood Test for FDI in Redundant Sensor Configurations," *Journal of Guidance and Control,* vol. 2, pp. 9-17, 1979.

[12] M. A. Sturza, "Navigation System Integrity Monitoring Using Redundant Measurements," *Journal of the Institute of Navigation,* vol. 35, 1988.

[13] A. Medvedev, "Fault Detection and Isolation by a Continuous Parity Space Method," *Automatica,* vol. 31, pp. 1039-1044, 1995.

[14] U. Krogmann, "Artificial Neural Networks for Inertial Sensor Fault Diagnosis," in *Symposium Gyro Technology*, Stuttgart, Germany, 1995.

[15] S. Feng, W. Y. Ochieng, D. Walsh, and R. Ioannides, "A measurement domain receiver autonomous integrity monitoring algorithm," *GPS Solutions,* vol. 10, pp. 85-96, 2006.

[16] A. J. Pejsa, "Optimum Skewed Redundant Inertial Navigators," *AIAA Journal,* vol. 12, pp. 899-902, 1974.

[17] A. Gelb, *Applied Optimal Estimation* vol. 14: MIT Press, 1994.

[18] J. Skaloud, J. Vallet, K. Keller, G. Veyssière, and O. Kölbl, "An Eye for Landscapes - Rapid Aerial Mapping with Handheld Sensors," *GPS World,* vol. May 2006, pp. 26-32, 2006.

[19] B. Southallzy, B. F. Buxtony, and J. A. Marchant, "Controllability and Observability: Tools for Kalman Filter Design," in *British Machine Vision Conference 98*, 1998, pp. 164-173.

[20] S. Hong, H.-H. Chun, S.-H. Kwon, and M. H. Lee, "Observability Measures and Their Application to GPS/INS," *IEEE Transaction on vehicular technology,* vol. 57, January 2008 2008.